

Selective population of spin-orbit levels in the autoionization of a polyatomic molecule: Branching ratios and asymmetry parameters for the Tanaka-Ogawa Rydberg series in CO₂

A. C. Parr

National Institute of Standards and Technology, Gaithersburg, Maryland 20899

P. M. Dehmer and J. L. Dehmer

Argonne National Laboratory, Argonne, Illinois 60439

K. Ueda,^{a)} J. B. West, M. R. F. Siggel, and M. A. Hayes

Daresbury Laboratory, Daresbury, Warrington WA4 4AD, United Kingdom

(Received 11 February 1994; accepted 11 March 1994)

The spin-orbit selectivity of angle-resolved photoelectron spectra was used to provide new information on the electronic structure, symmetry, and decay dynamics of members of the autoionizing Tanaka-Ogawa Rydberg series in CO₂. This represents the first time that spin-orbit selectivity has been used to obtain such information for a polyatomic molecule. The spin-orbit photoelectron branching ratios were used to show that the angular momentum quantum number λ of the excited Rydberg electron does not change upon autoionization. Furthermore, a consideration of the present results together with previous calculations of the relative intensities of the discrete and continuum ionization channels shows that the most probable electron configuration for the Tanaka-Ogawa Rydberg series is $\dots(\pi_u)^3(\pi_g)^4nd\delta_g$ and that autoionization proceeds primarily via a $d\delta_g \rightarrow \epsilon f\delta_u$ process for the totally symmetric vibronic components of the ion. The asymmetry parameter β was determined for individual spin-orbit components of the various vibronic bands of the $\tilde{X}^2\Pi_g$ state and is discussed in terms of recent theoretical calculations. The Rydberg series appears to be well described by $\Omega_c\omega$ coupling, even for relatively low principal quantum numbers. The general utility of this technique for autoionizing Rydberg states and its extension to multiphoton ionization of Rydberg states that lie below the first ionization threshold are discussed.

I. INTRODUCTION

The determination of the electronic structure, symmetry, and decay dynamics of Rydberg states is far more difficult for polyatomic molecules than for diatomic molecules. The definitive assignment of the symmetry of excited states has traditionally come from the rotational analysis of dipole transitions; however, for Rydberg states of polyatomic molecules and, particularly for those states that lie above the first ionization threshold, such as analysis is often impossible because the rotational structure is diffuse due to rapid decay of the state by ionization and dissociation. As a result, a number of alternative methods have been used to gain spectroscopic information on such states, including electron impact spectroscopy,¹ magnetic circular dichroism,² polarization-selected multiphoton processes,³⁻⁹ the observation of the polarization of fluorescence of photoions produced by autoionization of Rydberg states,¹⁰ and the comparison of such quantities as quantum defects and relative intensities of Rydberg series with theoretical predictions. The study of the decay dynamics of such states is likewise frustrated by the lack of rotational structure; studies are, by definition, rotationally averaged, and thus they provide far less information than studies in which all of the quantum numbers of both the excited state and the final state(s) are determined experimentally. Because diffuse rotational structure is an inherent char-

acteristic of polyatomic molecule spectra, alternative experimental probes that can provide insight into the properties of excited states are constantly being sought.

Recently, Guyon *et al.*¹¹ and Čubrić *et al.*^{12,13} have shown that information on the decay dynamics of autoionizing Rydberg states of diatomic molecules can be obtained when both the autoionizing state and the final ionic state show resolvable spin-orbit structure. In particular, they showed that for $^3\Pi_{\Omega=0,1,2}$ autoionizing Rydberg states of O₂, the relative populations of the O₂⁺ $X^2\Pi_{1/2g}$ and $X^2\Pi_{3/2g}$ spin-orbit components were strongly dependent on the value of Ω ; this dependence provided information on the angular momentum of the electron ejected in the autoionization process. In this paper, we demonstrate that this technique has significant potential for the study of autoionizing Rydberg states of polyatomic molecules, even for those states whose electronic structure and symmetry have not yet been well characterized, this by judicious combination of experimental observations and theoretical predictions. Here, we describe the first such study for the polyatomic molecule CO₂. We have determined both the spin-orbit branching ratios and the photoelectron angular distributions for individual spin-orbit components of the $\tilde{X}^2\Pi_g$ ionic ground state following the autoionization of a number of members of the Tanaka-Ogawa Rydberg series.

Because CO₂ is a first row, linear triatomic molecule and because it has been thoroughly studied, it is a logical initial choice for extension of the work of Guyon *et al.*¹¹ and Čubrić *et al.*^{12,13} There have been numerous investigations of the spectrum of CO₂ using both absorption¹⁴⁻²¹ and

^{a)}Permanent address: Research Institute for Scientific Measurements, Tohoku University, Sendai 980, Japan.

ionization^{22–30} techniques in the region of the prominent autoionization structure, i.e., in the region from the threshold for formation of $\tilde{X}^2\Pi_g$ (~ 900 Å) to the threshold for formation of $\tilde{C}^2\Sigma_g^+$ (~ 639 Å). The spectrum shows considerable discrete, diffuse structure. Much of this structure has been grouped into Rydberg series converging to the $\tilde{A}^2\Pi_u$, $\tilde{B}^2\Sigma_u^+$, and $\tilde{C}^2\Sigma_g^+$ states of the ion;^{16,17,31,32} these groupings were made almost exclusively on the basis of quantum defects and, in general, the electronic structures and the symmetries of the series are not known. The present investigation, which uses energy analysis of the ejected photoelectrons, is further aided by an excellent knowledge of the low-lying vibronic components of the $\tilde{X}^2\Pi_g$ ground state from fixed wavelength photoelectron spectroscopy,^{33–46} variable wavelength photoelectron spectroscopy,^{47–54} threshold photoelectron spectroscopy,^{55–59} zero kinetic energy photoelectron spectroscopy,^{60–61} and a variety of spectroscopic investigations of the ion.^{62–64} Some of these studies have also provided evidence for very high vibrational excitation of the ground state of the ion following autoionization of the Rydberg states in the ionization continuum.^{51,52,54} Indeed, the photoelectron spectra resulting from autoionization of the Tanaka–Ogawa bands extend for well over 1 eV. We also present here our first attempt at assigning some of these levels; however, a more complete discussion of the assignment of the higher vibronic levels, which will include Franck–Condon factor calculations, will be presented in a future paper.⁶⁵

There are strong similarities between the autoionization processes in the decay of the autoionizing states in O₂ (Refs. 11–13) and in CO₂. In both cases, the autoionizing Rydberg states have or are predicted to have $1,3\Pi_{\Omega=0,1,2}$ symmetry and the final ionic state has $2\Pi_{\Omega^+=1/2,3/2}$ symmetry. Thus, it is tempting to try to apply the $\Omega \rightarrow \Omega^+$ propensity rules derived and observed for O₂ to CO₂. However, we show here that this is not possible, because the Rydberg states in the two molecules are described by different Hund's coupling cases. In particular, the observed spin–orbit dependence of the branching ratios and asymmetry parameters depends critically on the coupling case for Rydberg states with $\Omega=1$.

II. SPECTROSCOPIC BACKGROUND

The ground state electron configuration of the linear CO₂ molecule is

$$(1\sigma_g)^2(1\sigma_u)^2(2\sigma_g)^2(3\sigma_g)^2(2\sigma_u)^2(4\sigma_g)^2 \\ \times (3\sigma_u)^2(1\pi_u)^4(1\pi_g)^4 \tilde{X}^1\Sigma_g^+$$

The present work focuses on a small region of the spectrum containing low-lying members of Rydberg series converging to the $\tilde{A}^2\Pi_u$ and $\tilde{B}^2\Sigma_u^+$ states of the ion. Because these ionic states are separated in energy by less than 1 eV,⁴⁶ strong perturbations occur between the ionic states and between the corresponding Rydberg series. This situation has added to the difficulty in making assignments.

The optically allowed transitions for series converging to the $\tilde{A}^2\Pi_u$ and $\tilde{B}^2\Sigma_u^+$ states of the ion in Hund's case (a) or (b) coupling (which are normally the appropriate coupling

cases for states of low principal quantum number) will be to states of $1\Sigma_u^+$ and $1\Pi_u$ symmetry;⁶⁶ the allowed series are

$$\text{CO}_2 \dots (4\sigma_g)^2(3\sigma_u)^2(1\pi_u)^4(1\pi_g)^4 \tilde{X}^1\Sigma_g^+ \\ \rightarrow (1\pi_u)^{-1}ns\sigma_g^1\Pi_u \\ \rightarrow (1\pi_u)^{-1}nd\sigma_g^1\Pi_u \\ \rightarrow (1\pi_u)^{-1}nd\pi_g^1\Sigma_u^+ \\ \rightarrow (1\pi_u)^{-1}nd\delta_g^1\Pi_u, \quad (1a)$$

$$\text{CO}_2 \dots (4\sigma_g)^2(3\sigma_u)^2(1\pi_u)^4(1\pi_g)^4 \tilde{X}^1\Sigma_g^+ \\ \rightarrow (3\sigma_u)^{-1}ns\sigma_g^1\Sigma_u^+ \\ \rightarrow (3\sigma_u)^{-1}nd\sigma_g^1\Sigma_u^+ \\ \rightarrow (3\sigma_u)^{-1}nd\pi_g^1\Pi_u. \quad (1b)$$

The optically allowed transitions in Hund's case (c) coupling, which is the appropriate coupling case for states of high principal quantum number or high rotational level, will be to states with $\Omega=0$ and 1; both such series are associated with each of the electron configurations listed earlier. The three normal vibrational modes in CO₂ associated with the neutral and the ionic states are denoted (ν_1, ν_2, ν_3), where ν_1 is the quantum number of the $\nu_1(\sigma_g^+)$ symmetric stretching mode; ν_2 is the quantum number of the $\nu_2(\pi_u)$ bending mode; and ν_3 is the quantum number of the $\nu_3(\sigma_u^+)$ asymmetric stretching mode.

Figure 1 shows the relative photoionization cross section for the production of CO₂⁺ from a rotationally cooled sample of CO₂ in the region of interest in the present study. These data were taken earlier³⁰ by using a high-intensity vacuum ultraviolet helium continuum light source, a 1 m near-normal incidence monochromator equipped with a 2400 line/mm grating, and a differentially pumped quadrupole mass filter for ion detection. With 25 μm entrance and exit slits, the observed wavelength resolution was 0.12 Å. The CO₂ sample gas was cooled by expanding a 10% mixture of CO₂ in Ar through an unskimmed 12.5 μm diameter jet with a stagnation pressure of 2000 Torr. Under these conditions, the beam temperature was estimated to be 20–25 K by using the method described previously.⁶⁷ This spectrum shows narrower autoionizing structure than does a similar spectrum taken at room temperature with a wavelength resolution of 0.07 Å,²⁸ and it serves as a useful visual aid for understanding the Rydberg structure of importance in the present study. The region shown contains the low-lying members of both the Tanaka–Ogawa Rydberg series¹⁷ that converge to $\tilde{A}^2\Pi_u$, $\nu_1^+=0-6$ and the Henning sharp and diffuse Rydberg series^{14,16,17} that converge to $\tilde{B}^2\Sigma_u^+$, $\nu_1^+=0$. The $n=3$ member of the Henning sharp series, the most intense peak in the photoionization spectrum, has an intensity of 50 on the scale of Fig. 1.

Although the present work focuses on the Tanaka–Ogawa series, it is useful to review the current understanding of the electron configurations and the symmetries of all three series, since the series may be mutually perturbing. Most simply, the series could be assigned to three of the $n/l\lambda$ electron configurations given in Eq. (1); however, this is may

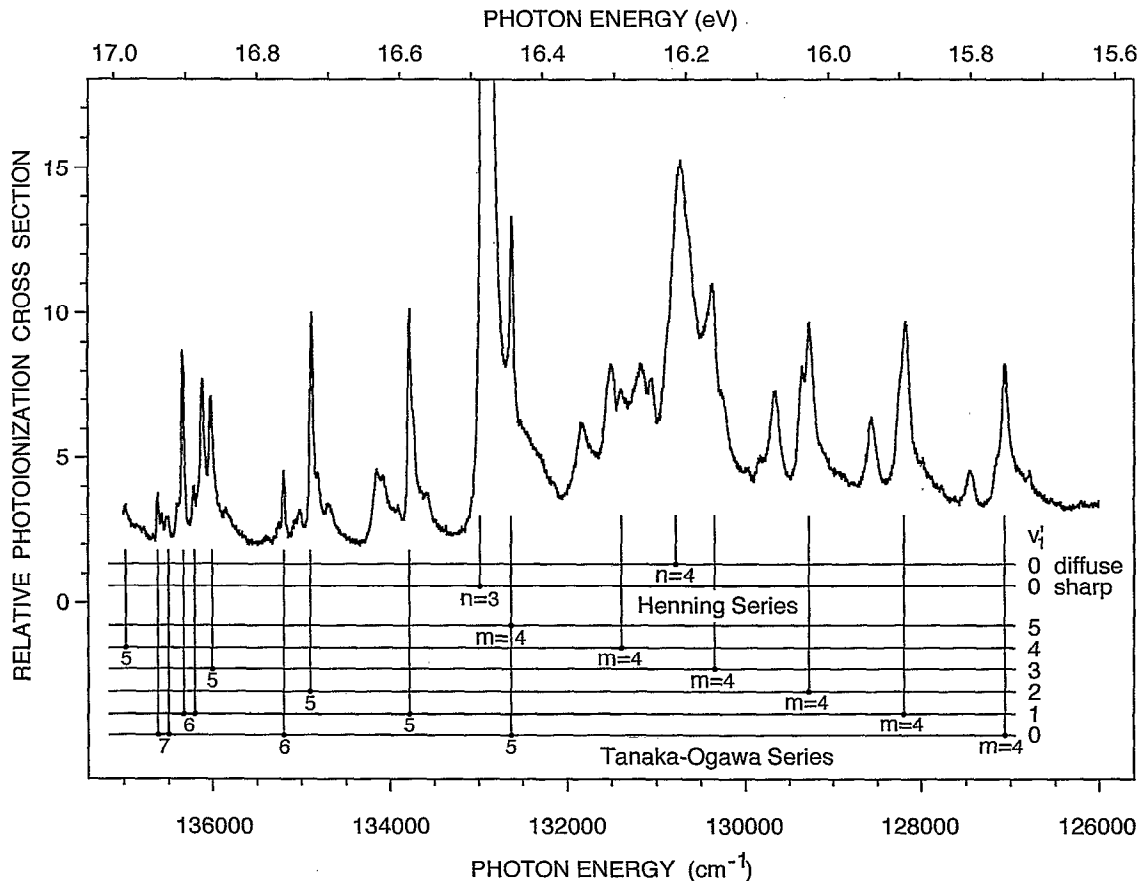


FIG. 1. Relative photoionization cross section for rotationally cooled CO₂ determined at a wavelength resolution of 0.12 Å. The $n=3$ member of the Henning series has an intensity of 50 on the scale of this figure.

well be unrealistic both because l is not a good quantum number in molecules and because case (a) or (b) coupling may not be appropriate for these series. Nevertheless, it is useful to begin with this model.

The Henning sharp and diffuse series are considerably better understood than the Tanaka–Ogawa series. These two series must correlate with two of the three electron configurations given in Eq. (1b). There is now nearly uniform agreement that the Henning diffuse series corresponds to $ns\sigma_g^1\Sigma_u^+$. The observed quantum defect ($\delta \sim 0.3, \text{ mod } 1$) is in accord with the calculations of Fridh *et al.*³² England and Ermler,⁶⁸ Padiál *et al.*,⁶⁹ and Dittman *et al.*⁷⁰ Furthermore, the results of Poliakoff *et al.*¹⁰ on the determination of the polarization of fluorescence from the CO₂⁺ $\tilde{X}^2\Pi_g \leftarrow \tilde{A}^2\Pi_u$ transition following autoionization of the Henning sharp and diffuse series show that both series have $^1\Sigma_u^+$ character. Somewhat more controversy surrounds the assignment of the Henning sharp series, which has $\delta \sim 0.0, \text{ mod } 1$. Fridh *et al.*³² assigned the Henning sharp series as $nd\pi_g^1\Pi_u$; however, Padiál *et al.*⁶⁹ and Dittman *et al.*⁷⁰ showed that the $nd\pi_g$ excitation is too weak to account for the large intensity of the Henning sharp series. England and Ermler⁶⁸ assigned the Henning sharp series as $nd\sigma_g^1\Sigma_u^+$ in accord with the results of Poliakoff *et al.*,¹⁰ which show that this series has $^1\Sigma_u^+$ character. Thus, the most probable assignments appear to be as follows: The Henning diffuse series is $ns\sigma_g^1\Sigma_u^+$, and the

Henning sharp series is $nd\sigma_g^1\Sigma_u^+$. Members of these series shown in Fig. 1 are labeled with their principal quantum numbers, n ; this modifies the assignments originally proposed by Lindholm³¹ and retained in other, more recent, works even though the diffuse series was reassigned some time ago.³²

Less is known about the Tanaka–Ogawa series, which has $\delta \sim 0.06, \text{ mod } 1$. The most intense members of this series converge to $\tilde{A}^2\Pi_{1/2u}$; considerably weaker members converge to $\tilde{A}^2\Pi_{3/2u}$. Fridh *et al.*³² assigned this series as $ns\sigma_g^1\Pi_u$ and predicted that the lowest member of this series, the $n=3$ member, would lie near the first ionization threshold. The $3s\sigma_g^1\Pi_u$ state has recently been identified in the high resolution absorption spectrum⁷¹ and has $\delta = 1.2$, in rather poor agreement with the quantum defect of the Tanaka–Ogawa series. However, other evidence suggests that the Tanaka–Ogawa series is an nd series. England and Ermler⁶⁸ assigned the series as $nd\delta_g^1\Pi_u$. In addition, Padiál *et al.*⁶⁹ and Dittman *et al.*⁷⁰ have shown that the σ_g channel is strong only for the lowest transition, which is the transition to $5\sigma_g$. The notation $5\sigma_g$ is preferred to $3s\sigma_g$, because $5\sigma_g$ is a mixed-character orbital rather than a Rydberg orbital.⁷² Because the $5\sigma_g$ state is not a true Rydberg orbital, its quantum defect need not agree with that of higher members of the $ns\sigma_g$ series. In the region of interest in the present work, the calculations indicate that the δ_g channel is

considerably more intense than the σ_g channel because of the effects of a shape resonance. Both calculations^{69,70} indicate that the π_g channel is far too weak to account for the observed series. Therefore, to summarize, we can eliminate the $nd\pi_g\ ^1\Sigma_u^+$ transition from further consideration, because it is predicted to be extremely weak. Furthermore, the weight of the theoretical evidence (calculations of both intensity and quantum defects) indicates that the $nd\delta_g\ ^1\Pi_u$ configuration is more probable than either the $ns\sigma_g$ or $nd\sigma_g$ configurations. Here, we seek to confirm these recent theoretical predictions, if possible, and to understand the decay dynamics of members of the Tanaka–Ogawa Rydberg series. Members of this series shown in Fig. 1 are labeled with the running number, m , corresponding to the conventional number in use to date. The relationship of m to the true principal quantum number n is $n=m-1$ if the series is $nd\delta_g$ (as predicted by theory) or $nd\sigma_g$; however, the relationship is $n=m$ if the series is $ns\sigma_g$.

III. EXPERIMENTAL APPARATUS AND RESULTS

A. Experimental apparatus

The electron spectrometer system used in this study comprised two hemispherical electron analyzers, each positioned to detect electrons ejected at right angles relative to the horizontal photon beam. One analyzer was fixed in position and accepted electrons ejected horizontally; the other was rotatable about the light beam through an angular range of a little more than 90° from a vertical orientation. The angular acceptance of each analyzer was limited by an aperture in the entrance lens to approximately $\pm 2^\circ$. With a pass energy of 1 eV, the electron resolution was ~ 17 meV. To enhance the sensitivity of the spectrometers, area detectors of the resistive anode type were mounted at the exit plane of the hemispheres. A complete description of the electron spectrometer system has been published previously by Parr *et al.*⁷³

A 2 mm i.d. capillary light guide channeled the vacuum ultraviolet radiation from the exit slit of the optical monochromator to a point near the gas outlet to form an ionization region “viewed” by both analyzers. The vacuum ultraviolet radiation was provided by the Synchrotron Radiation Source at Daresbury Laboratory, a 2 GeV electron storage ring. Light was focused onto the entrance slit of a 5 m near-normal-incidence monochromator; in the present experiments, the wavelength resolution was ~ 0.25 Å (~ 6 meV). The normal-incidence monochromator and its performance have been described by Holland *et al.*,⁷⁴ and the beamline to which this instrument was attached has been described by West and Padmore.⁷⁵

The CO₂ sample gas was cooled by expanding pure CO₂ through an unskimmed 25 μ m diameter jet at a stagnation pressure of 1.067×10^5 Pa; the jet tip was positioned 3 mm from the ionization region. Under these expansion conditions, the ionization rate for the dimer was 2% that for the monomer, and the ionization rate for heavier clusters was negligible.⁷⁶ The pressure in the ionization region during the measurements was $\sim 4.0 \times 10^{-3}$ Pa. The beam temperature was estimated to be 20 K,⁶⁷ which is approximately the same

as that for the data shown in Fig. 1; however, the actual beam temperature was apparently somewhat higher as evidence by the observed linewidths, which appeared broader than those in Fig. 1.

The radiation from the exit slit of the monochromator was elliptically polarized with the major axis of the ellipse in the horizontal plane. The degree of polarization was determined by using an analyzer incorporating three gold coated mirrors that was attached to the rotating analyzer. The transmission function (or detection efficiency) of each electron spectrometer was determined as a function of the photoelectron energy by using the known photoionization cross sections⁷⁷ and angular distributions⁷⁸ for Ar. The electron signal was corrected for the variation of incident light flux, which was measured by an incident flux monitor, a tungsten mesh in the polarization analyzer. The angular distribution of the photoelectrons for dipole excitation of randomly oriented molecules is given by the expression⁷⁹

$$\frac{d\sigma}{d\Omega} = \frac{\sigma}{4\pi} \left(1 + \frac{\beta}{4} (3p \cos 2\theta + 1) \right), \quad (2)$$

where the photoelectron asymmetry parameter β completely characterizes the photoelectron angular distribution. In this expression, p is the polarization of the incoming light, θ is the angle between the major polarization axis and the ejected electron direction, and σ is the partial cross section for that channel. This expression was used for calibration and to determine the values of the partial cross section σ and the asymmetry parameter β .

B. Photoelectron spectra and angular distributions

Photoelectron spectra were obtained for the following autoionizing bands shown in Fig. 1: (1) the $n=3$, (000) member of the Henning sharp series at $132\,977\text{ cm}^{-1}$; (2) the $m=5$, (100) member of the Tanaka–Ogawa series at $133\,779\text{ cm}^{-1}$; (3) the entire energy region $\sim 134\,725$ – $135\,210\text{ cm}^{-1}$ at intervals of 32 cm^{-1} , which includes the $m=5$, (200) member of the Tanaka–Ogawa series at $134\,899\text{ cm}^{-1}$ and the $m=6$, (000) member of the Tanaka–Ogawa series at $135\,193\text{ cm}^{-1}$; and (4) the unassigned peak at $\sim 136\,108\text{ cm}^{-1}$. As expected (because the $\tilde{B}^2\Sigma_u^+$ ion core does not show spin–orbit splitting), the photoelectron spectrum taken on the $n=3$, (000) member of the Henning sharp series at $132\,977\text{ cm}^{-1}$ shows equal branching ratios for the formation of $\tilde{X}^2\Pi_{3/2g}$ and $\tilde{X}^2\Pi_{1/2g}$. So, too, does the photoelectron spectrum taken on the unassigned band. However, the photoelectron spectra taken at energies corresponding to members of the Tanaka–Ogawa series all show substantial enhancement in the intensity of the $^2\Pi_{1/2g}$ spin–orbit component in each totally symmetric photoelectron band.

In this paper, we concentrate on the $m=5$, (200) member of the Tanaka–Ogawa series at $134\,899\text{ cm}^{-1}$. Photoelectron spectra were taken across this band; hence, it is possible to estimate the contribution to each photoelectron peak from continuum ionization. (This is because the bands in the Tanaka–Ogawa Rydberg series have large Fano q parameters, suggesting that the interactions between the discrete autoionizing resonances and the underlying continua are

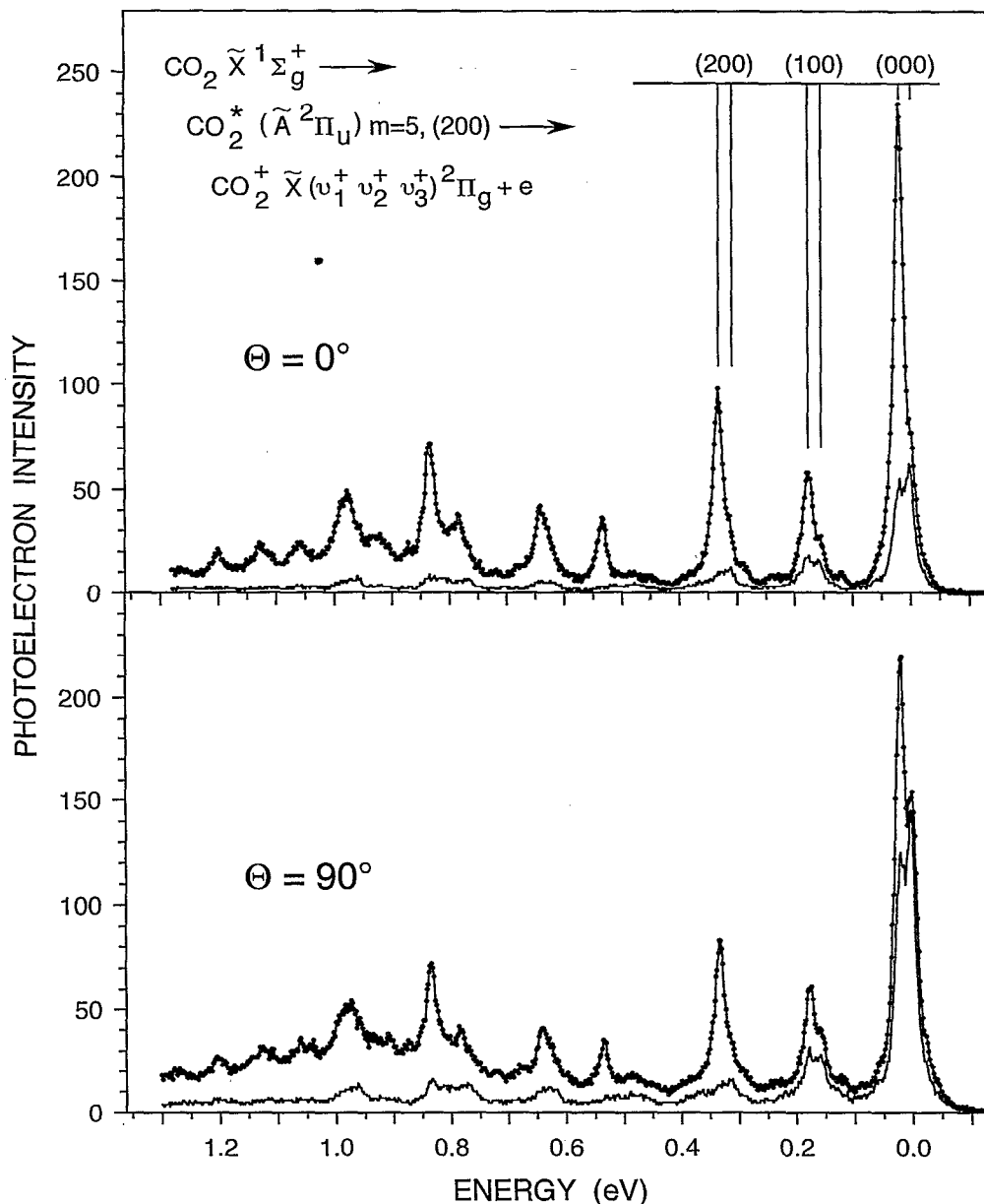


FIG. 2. Photoelectron spectra taken on the $m=5, (200)$ member of the Tanaka–Ogawa series at 0° and 90° . The spectra with the solid data points were taken on resonance; those spectra without data points were taken off resonance. The energy scale is with respect to the $\tilde{X}(000)^2\Pi_{3/2g}$ level.

weak.) Figure 2 shows photoelectron spectra taken at 0° (upper panel) and 90° (lower panel) both on resonance ($134\,899\text{ cm}^{-1}$) and off resonance (at $134\,996\text{ cm}^{-1}$, the minimum on the high energy side of the autoionizing peak). Figure 3 shows the difference between the on-resonance and off-resonance photoelectron spectra for the data taken at 0° . This difference spectrum is exceptionally striking, showing that virtually 100% of the photoelectron intensity appears in the $^2\Pi_{1/2g}$ spin-orbit component for each assigned totally symmetric vibronic band. Figure 4 shows the photoelectron asymmetry parameter β as a function of excitation energy for both the $\tilde{X}(000)^2\Pi_{3/2g}$ and $\tilde{X}(000)^2\Pi_{1/2g}$ photoelectron bands and the relevant region of the total photoionization cross section from Fig. 1. (The difference in widths of these two spectra results from the difference in rotational tempera-

ture of the molecular beams and from the difference in wavelength resolution in the two spectra.) It is not possible to separate the contributions from resonance and continuum ionization for the quantity β .

IV. DISCUSSION

A. Assignment of the bands in the photoelectron spectrum

The present discussion is limited to the assignment of the prominent bands in the energy region of the photoelectron spectrum shown in Fig. 3, which is the difference between the on-resonance and the off-resonance photoelectron spectra for the $m=5, (200)$ member of the Tanaka–Ogawa series. The many weak features and the features at higher

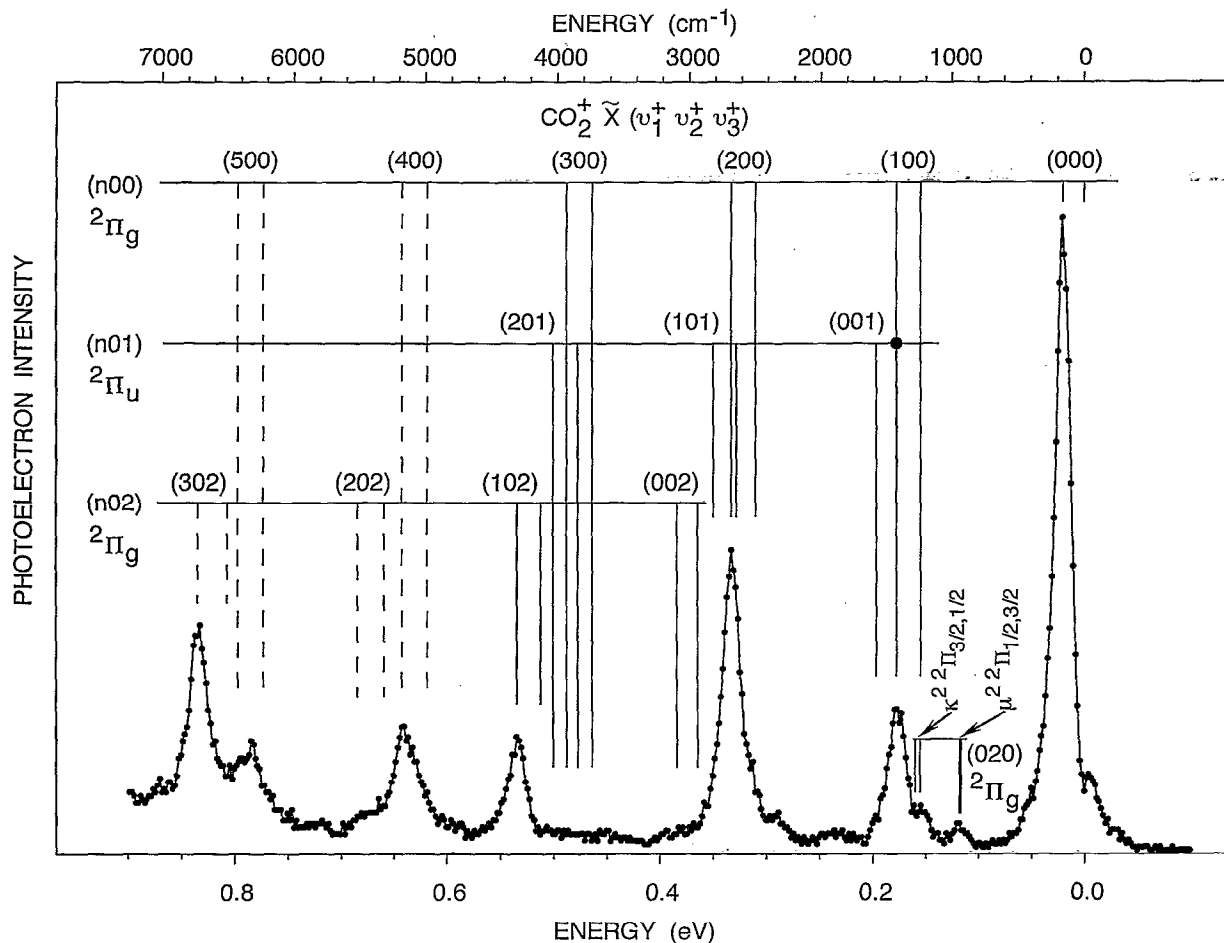


FIG. 3. Photoelectron spectrum taken on the $m=5$, (200) member of the Tanaka–Ogawa series at 0° (difference between the on-resonance and off-resonance spectra of Fig. 2). The known energy levels of members of the $(\nu_1 00)$, $(\nu_1 01)$, and $(\nu_1 02)$ progressions are shown as solid lines (Ref. 62); higher members of these progressions, which were estimated by linear or quadratic extrapolation of the known levels, are shown as dashed lines. The energy scales are with respect to the $\tilde{X}(000)^2\Pi_{3/2g}$ level.

energy will be discussed in a future paper.⁶⁵ The known energy levels⁶² of members of the $(\nu_1 00)$, $(\nu_1 01)$, and $(\nu_1 02)$ progressions are shown in Fig. 3 as solid lines; higher members of these progressions, which were estimated by linear or quadratic extrapolation of the known levels, are shown as dashed lines. The vibronic symmetry of each progression is shown below the progression label; for example, the $(\nu_1 00)$ progression has $^2\Pi_g$ vibronic symmetry.

Table I presents the observed energies and our assignments for the six prominent bands in the spectrum. We have assigned the three lowest energy bands as the three lowest members of the $\tilde{X}(\nu_1 00)^2\Pi_{1/2g}$ progression on the basis of their observed energies and the uniformity of their observed asymmetry parameters. Although there is a near coincidence in energy between the $\tilde{X}(100)^2\Pi_{1/2g}$ and $\tilde{X}(001)^2\Pi_{3/2g}$ levels and between the $\tilde{X}(200)^2\Pi_{1/2g}$ and $\tilde{X}(101)^2\Pi_{3/2g}$ levels, the $(\nu_1 00)$ and $(\nu_1 01)$ progressions are expected to have different asymmetry parameters, because the autoionization process must necessarily be different for the progressions. The $(\nu_1 00)$ progression has gerade vibronic symmetry and must result from the ejection of an ungerade electron during the autoionizing process, while the $(\nu_1 01)$ progression has ungerade vibronic symmetry and must result from the

ejection of a gerade electron during the autoionizing process. Although these two processes might result in photoelectrons that have the same value of β , it is unlikely that they do. We note that the $n=3$ member of the Henning sharp Rydberg series autoionizes to produce a strong $\tilde{X}(000)^2\Pi_g$ band and significant $\tilde{X}(001)^2\Pi_u$ and $\tilde{X}(101)^2\Pi_u$ bands; the asymmetry parameter for the (000) band is quite different from that of the $(\nu_1 01)$ bands.⁶⁵

We have assigned the two highest energy bands in Fig. 3 by extrapolation of the known energy levels; these bands are the $\tilde{X}(400)^2\Pi_{1/2g}$ level at 5174.1 cm^{-1} and the $\tilde{X}(302)^2\Pi_{1/2g}$ level at 6727.7 cm^{-1} . The $\tilde{X}(400)^2\Pi_{1/2g}$ band is broader than the electron spectrometer resolution and is degraded toward lower energy, indicating that it contains contributions from additional photoelectron bands.

Our assignments indicate that the most intense vibronic levels populated by autoionization of the $m=5$, (200) member of the Tanaka–Ogawa series have gerade vibronic symmetry and can be attributed to $\tilde{X}(\nu_1 00)^2\Pi_{1/2g}$ and $\tilde{X}(\nu_1 02)^2\Pi_{1/2g}$ levels. No bands with ungerade vibronic symmetry (odd quanta of the bending or asymmetric stretching modes) have been identified. The photoelectron spectrum for the $m=5$, (100) member of the Tanaka–Ogawa series

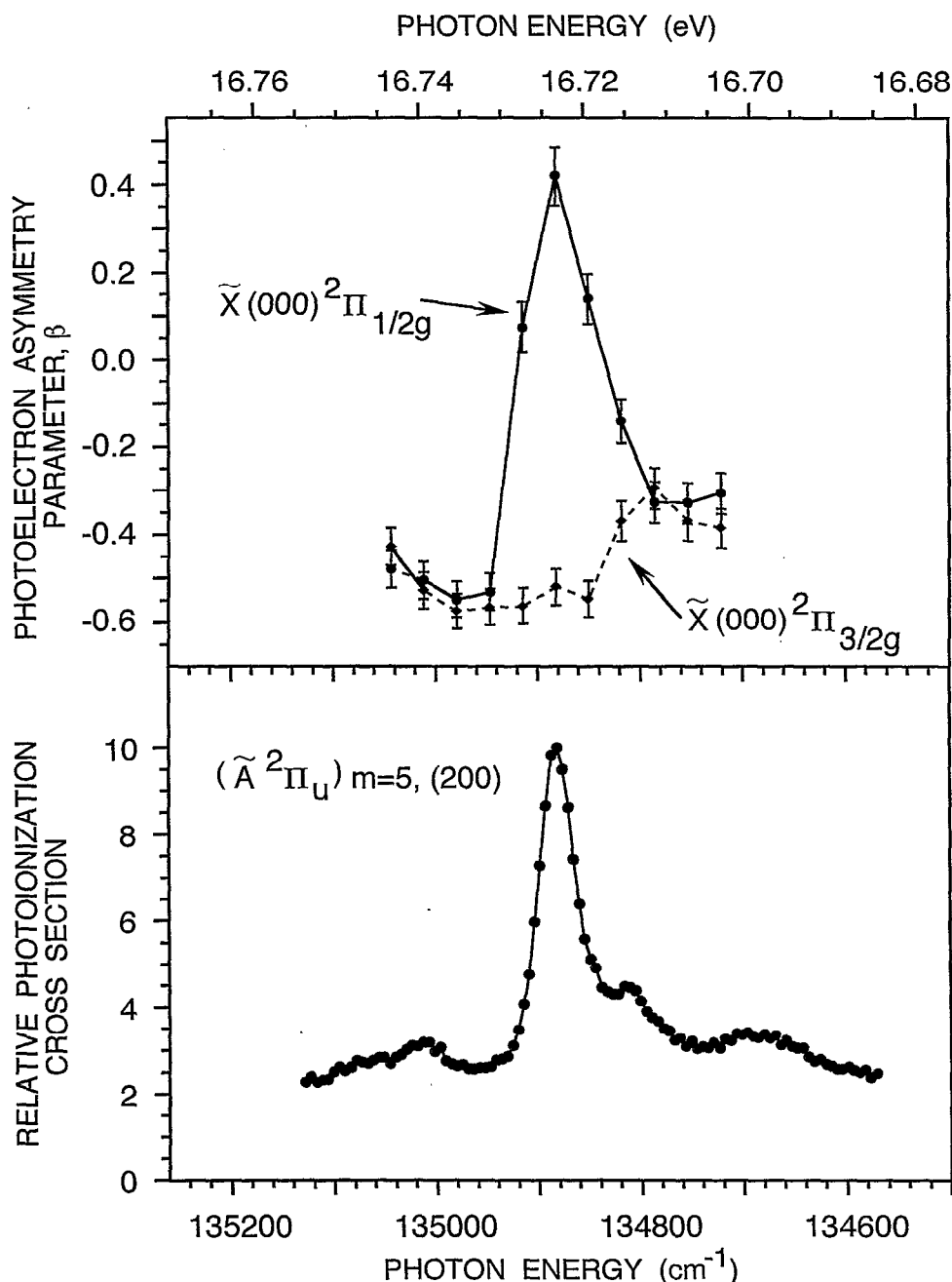


FIG. 4. Wavelength dependence of the photoelectron asymmetry parameter β for production of $\tilde{X}(000)^2\Pi_{1/2g}$ and $\tilde{X}(000)^2\Pi_{3/2g}$ (upper panel) and the relative photoionization cross section from Fig. 1 (lower panel) in the region of the $m=5, (200)$ member of the Tanaka–Ogawa series. The difference in widths of the resonance in the two frames is due to the difference in rotational temperature in the molecular beams used for the two sets of data and to the difference in wavelength resolution for the two sets of data.

shows structure somewhat different from that for the $m=5, (200)$ member shown in Fig. 3; however, the prominent bands also are of gerade symmetry. Hence, the following discussion is limited to autoionization processes in which an ungerade electron is ejected to produce a final ionic state with overall gerade symmetry.

B. Selective population of spin–orbit levels

The population of spin–orbit levels is determined solely by the selection rules for autoionization, which are exactly

those for a homogeneous perturbation, that is, the excited Rydberg state and the ion plus outgoing electron must obey the following: $\Delta S = \Delta L = \Delta J = \Delta \Omega = 0$. Depending on the Hund's coupling case, some of these may not apply. Guyon *et al.*¹¹ and Čubrić *et al.*¹³ have published tables showing possible combinations of excited states and continuum states that obey these rules for autoionization of O₂ assuming Hund's case (a) or (b) coupling. We have adapted and expanded these tables for CO₂ in order to show quantum numbers appropriate both to case (a) or (b) coupling and to case

TABLE I. Observed energies of the prominent bands in the photoelectron spectrum of the Tanaka–Ogawa $m=5$, (200) band.

Observed energy (cm ⁻¹)	Other experimental energy ^a (cm ⁻¹)	Extrapolated energy (cm ⁻¹)	Assignment
156.4	159.33		$\tilde{X}(000)^2\Pi_{1/2g}$
1421.5	1425.1		$\tilde{X}(100)^2\Pi_{1/2g}$
2682.4	2680.3		$\tilde{X}(200)^2\Pi_{1/2g}$
4305.7	4306.5		$\tilde{X}(102)^2\Pi_{1/2g}$
5174.1		~5180 ^b	$\tilde{X}(400)^2\Pi_{1/2g}$
6727.7		~6729 ^c	$\tilde{X}(302)^2\Pi_{1/2g}$

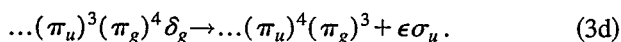
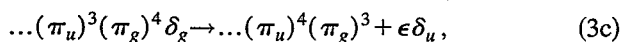
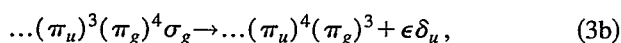
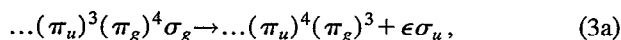
^aReference 62.

^bA linear or quadratic extrapolation of the energies of the $\tilde{X}(000)^2\Pi_{3/2g}$ levels places the $\tilde{X}(400)^2\Pi_{3/2g}$ level at 4987 cm⁻¹; assuming that the spin–orbit splitting of the (400) level is the same as that of the (300) level, then the $\tilde{X}(000)^2\Pi_{1/2g}$ level is estimated to be at 5180 cm⁻¹.

^cFrom a linear extrapolation of the $\tilde{X}(v_1 0 2)^2\Pi_{1/2g}$ levels.

(c) coupling (hereafter referred to as ΛS coupling and $\Omega_c\omega$ coupling, respectively⁸⁰). The results are shown in Table II. Both singlet and triplet states are included to facilitate the discussion of the transition from ΛS coupling to $\Omega_c\omega$ coupling. Note that implicit in Table II is the assumption that the spin of the excited electron does not change upon autoionization, i.e., that $\sigma_R = \sigma_e$ and that $\sigma_c = \sigma^+$, where σ_R , σ_e , σ_c , and σ^+ are the projections on the internuclear axis of the spin angular momenta of the Rydberg electron, the ejected electron, the core electrons before autoionization, and the core electrons following autoionization, respectively. This assumption is reasonable, since both the ionic state to which the Tanaka–Ogawa series converges ($\tilde{A}^2\Pi_u$) and the final ionic state after autoionization ($\tilde{X}^2\Pi_g$) have the same spin multiplicity.

Table II is limited to only four autoionization processes, because (1) as noted earlier, all of the theoretical calculations indicate that the Tanaka–Ogawa series most probably results from an $nd\delta_g$ or, possibly, an $ns\sigma_g$ excitation, (2) the photoelectron spectra show that the final ionic state has overall gerade symmetry, requiring the ejection of an ungerade electron, (3) dipole selection rules limit transitions to Rydberg state having $^1\Sigma_u^+$ and $^1\Pi_u$ symmetry in ΛS coupling or $\Omega=0$ or 1 symmetry in $\Omega_c\omega$ coupling, and (4) the overall symmetry of the Rydberg state and the complex composed of the ion $\dots(\pi_g)^3$ plus the outgoing electron $\epsilon\lambda_u$ must be conserved. The four combinations of Rydberg state configuration and ion plus outgoing electron that satisfy these requirements are the following:



In order to use the information in Table II, it is necessary to understand how the $\Omega=1$ levels behave in ΛS coupling and in $\Omega_c\omega$ coupling. Following Lefebvre-Brion and Field,⁸¹ the wave functions are written in the form $|\lambda_c, \sigma_c, \lambda_R, \sigma_R\rangle$.

For the case of the $\dots(\pi_u)^3(\pi_g)^4\sigma_g$ configuration, the wave functions in ΛS coupling (ignoring full or half-full orbitals) are

$$^3\Pi_2 = | +1, +1/2, 0, +1/2 \rangle, \quad (4a)$$

$$^3\Pi_1 = \frac{1}{\sqrt{2}} \{ | +1, +1/2, 0, -1/2 \rangle + | +1, -1/2, 0, +1/2 \rangle \}, \quad (4b)$$

$$^3\Pi_0 = | +1, -1/2, 0, -1/2 \rangle, \quad (4c)$$

$$^1\Pi_1 = \frac{1}{\sqrt{2}} \{ | +1, +1/2, 0, -1/2 \rangle - | +1, -1/2, 0, +1/2 \rangle \}. \quad (4d)$$

These functions are equivalent to those shown in the appendix of Čubrić *et al.*¹³ As is seen, in ΛS coupling the $\Omega=0$ and 2 levels have pure $\tilde{A}^2\Pi_{1/2u}$ and $\tilde{A}^2\Pi_{3/2u}$ cores, respectively; but the $\Omega=1$ levels result from a linear combination of the $\tilde{A}^2\Pi_{1/2u}$ and the $\tilde{A}^2\Pi_{3/2u}$ core states. However, in $\Omega_c\omega$ coupling, this is not the case. The $\Omega=1$ levels given in Eqs. (4b) and (4d) are completely mixed to produce two new functions denoted 1^+ and 1^- , which are given by

$$1^+ = \frac{1}{\sqrt{2}} \{ |^3\Pi_1\rangle + |^1\Pi_1\rangle \} = | +1, +1/2, 0, -1/2 \rangle, \quad (5a)$$

$$1^- = \frac{1}{\sqrt{2}} \{ |^3\Pi_1\rangle - |^1\Pi_1\rangle \} = | +1, -1/2, 0, +1/2 \rangle. \quad (5b)$$

Here, the 1^+ function has only the $\tilde{A}^2\Pi_{3/2u}$ core, and the 1^- function has only the $\tilde{A}^2\Pi_{1/2u}$ core. Analogous functions can be written for the $\dots(\pi_u)^3(\pi_g)^4\delta_g$ configuration. This change in the description of the $\Omega=1$ levels reflects the transition from ΛS coupling, in which the Rydberg electron is strongly coupled to the core electrons by exchange effects, to $\Omega_c\omega$ coupling, in which the Rydberg electron is strongly coupled to one of the two spin–orbit states of the ion core.

By using the information from Table II and from Eqs. (4) and (5), selection rules may be determined for $\Omega_c \rightarrow \Omega^+$ for autoionization of a Rydberg state in either ΛS coupling or $\Omega_c\omega$ coupling. The results are given in Table III.

The observation by Tanaka and Ogawa that the intense members of the Tanaka–Ogawa series converge to the $\tilde{A}^2\Pi_{1/2u}$ ion core combined with the present observation that members of this series autoionize to produce the $\tilde{X}^2\Pi_{1/2u}$ ion core greatly limits the combinations of allowed configurations of excited state and ion core plus outgoing electron. Table III shows that only three dipole-allowed possibilities exist for the $\Omega_c = \frac{1}{2} \rightarrow \Omega^+ = \frac{1}{2}$ process. These are that (1) the Rydberg state is $^3\Pi_0$ in ΛS coupling (equivalent to $\Omega=0$ in $\Omega_c\omega$ coupling) for autoionization via $\sigma_g \rightarrow \epsilon\sigma_u$; (2) the Rydberg state is $\Omega=1^-$ in $\Omega_c\omega$ coupling for autoionization via $\sigma_g \rightarrow \epsilon\sigma_u$; (3) the Rydberg state is $\Omega=1^-$ in $\Omega_c\omega$ coupling for autoionization via $\delta_g \rightarrow \epsilon\delta_u$. The transition from $\tilde{X}^1\Sigma_g^+$ to $^3\Pi_0$ is forbidden in ΛS coupling, and it would be expected to be weak or absent if this were the appropriate coupling case. The remaining possibilities require that the excited state be described by $\Omega_c\omega$ coupling. While one

TABLE II. Symmetry considerations for autoionization of the Tanaka-Ogawa series, i.e., for transitions of the type CO₂ $\tilde{X}^1\Sigma_g^+ \rightarrow \text{CO}_2^*(\tilde{A}^2\Pi_u)n\lambda_R \rightarrow \text{CO}_2^+(\tilde{X}^2\Pi_g) + \epsilon\lambda_e$.

Rydberg state to continuum state transition	Rydberg state label		Rydberg state core		Rydberg state electron		Rydberg state quantum numbers					Ion state core following autoionization			Outgoing electron		Ion core quantum numbers			
	Case (a)	Case (b)	λ_c	σ_c	Core state	λ_R	σ_R	Case (a) or (b)			Case (c)		λ^+	σ^+	Ion state	λ_e	σ_e	Ω^+	ω_e	
	or (b)	(c)						Σ	Λ	Ω	Ω_c	ω_R								
$(\pi_u)^3(\pi_g)^4\sigma_g \rightarrow (\pi_u)^4(\pi_g)^3 + \epsilon\sigma_u$	$^3\Pi_{2u}$	$\Omega=2$	+1	$+\frac{1}{2}$	$\tilde{A}^2\Pi_{3/2u}$	0	$+\frac{1}{2}$	+1	+1	+2	$+\frac{3}{2}$	$+\frac{1}{2}$	+1	$+\frac{1}{2}$	$\tilde{X}^2\Pi_{3/2g}$	0	$+\frac{1}{2}$	$+\frac{3}{2}$	$+\frac{1}{2}$	
			-1	$-\frac{1}{2}$	$\tilde{A}^2\Pi_{3/2u}$	0	$-\frac{1}{2}$	-1	-1	-2	$-\frac{3}{2}$	$-\frac{1}{2}$	-1	$-\frac{1}{2}$	$\tilde{X}^2\Pi_{3/2g}$	0	$-\frac{1}{2}$	$-\frac{3}{2}$	$-\frac{1}{2}$	
		+1	$-\frac{1}{2}$	$\tilde{A}^2\Pi_{1/2u}$	0	$+\frac{1}{2}$	0	+1	+1	$+\frac{1}{2}$	$+\frac{1}{2}$	+1	$-\frac{1}{2}$	$\tilde{X}^2\Pi_{1/2g}$	0	$+\frac{1}{2}$	$+\frac{1}{2}$	$+\frac{1}{2}$		
		-1	$-\frac{1}{2}$	$\tilde{A}^2\Pi_{3/2u}$	0	$+\frac{1}{2}$	0	-1	-1	$-\frac{3}{2}$	$+\frac{1}{2}$	-1	$-\frac{1}{2}$	$\tilde{X}^2\Pi_{3/2g}$	0	$+\frac{1}{2}$	$-\frac{3}{2}$	$+\frac{1}{2}$		
		-1	$+\frac{1}{2}$	$\tilde{A}^2\Pi_{1/2u}$	0	$-\frac{1}{2}$	0	-1	-1	$-\frac{1}{2}$	$-\frac{1}{2}$	-1	$+\frac{1}{2}$	$\tilde{X}^2\Pi_{1/2g}$	0	$-\frac{1}{2}$	$-\frac{1}{2}$	$-\frac{1}{2}$		
		+1	$-\frac{1}{2}$	$\tilde{A}^2\Pi_{1/2u}$	0	$-\frac{1}{2}$	-1	+1	0	$+\frac{1}{2}$	$-\frac{1}{2}$	+1	$-\frac{1}{2}$	$\tilde{X}^2\Pi_{1/2g}$	0	$-\frac{1}{2}$	$+\frac{1}{2}$	$-\frac{1}{2}$		
	$(\pi_u)^3(\pi_g)^4\sigma_g \rightarrow (\pi_u)^4(\pi_g)^3 + \epsilon\delta_u$	$^3\Pi_{2u}$	$\Omega=2$	+1	$+\frac{1}{2}$	$\tilde{A}^2\Pi_{3/2u}$	0	$+\frac{1}{2}$	+1	+1	+2	$+\frac{3}{2}$	$+\frac{1}{2}$	-1	$+\frac{1}{2}$	$\tilde{X}^2\Pi_{1/2g}$	+2	$+\frac{1}{2}$	$-\frac{1}{2}$	$+\frac{5}{2}$
				-1	$-\frac{1}{2}$	$\tilde{A}^2\Pi_{3/2u}$	0	$-\frac{1}{2}$	-1	-1	+2	$-\frac{3}{2}$	$-\frac{1}{2}$	+1	$-\frac{1}{2}$	$\tilde{X}^2\Pi_{1/2g}$	-2	$-\frac{1}{2}$	$+\frac{1}{2}$	$-\frac{5}{2}$
			+1	$-\frac{1}{2}$	$\tilde{A}^2\Pi_{1/2u}$	0	$+\frac{1}{2}$	0	+1	+1	$+\frac{1}{2}$	$+\frac{1}{2}$	-1	$-\frac{1}{2}$	$\tilde{X}^2\Pi_{3/2g}$	+2	$+\frac{1}{2}$	$-\frac{3}{2}$	$+\frac{5}{2}$	
			-1	$-\frac{1}{2}$	$\tilde{A}^2\Pi_{3/2u}$	0	$+\frac{1}{2}$	0	-1	-1	$-\frac{3}{2}$	$+\frac{1}{2}$	+1	$-\frac{1}{2}$	$\tilde{X}^2\Pi_{1/2g}$	-2	$+\frac{1}{2}$	$+\frac{1}{2}$	$-\frac{3}{2}$	
			-1	$+\frac{1}{2}$	$\tilde{A}^2\Pi_{1/2u}$	0	$-\frac{1}{2}$	0	-1	-1	$-\frac{1}{2}$	$-\frac{1}{2}$	+1	$+\frac{1}{2}$	$\tilde{X}^2\Pi_{3/2g}$	-2	$-\frac{1}{2}$	$+\frac{3}{2}$	$-\frac{5}{2}$	
			+1	$-\frac{1}{2}$	$\tilde{A}^2\Pi_{1/2u}$	0	$-\frac{1}{2}$	-1	+1	0	$+\frac{1}{2}$	$-\frac{1}{2}$	-1	$-\frac{1}{2}$	$\tilde{X}^2\Pi_{3/2g}$	+2	$-\frac{1}{2}$	$-\frac{3}{2}$	$+\frac{3}{2}$	
$(\pi_u)^3(\pi_g)^4\delta_g \rightarrow (\pi_u)^4(\pi_g)^3 + \epsilon\sigma_u$		$^3\Pi_{2u}$	$\Omega=2$	-1	$+\frac{1}{2}$	$\tilde{A}^2\Pi_{1/2u}$	+2	$+\frac{1}{2}$	+1	+1	+2	$-\frac{1}{2}$	$+\frac{5}{2}$	+1	$+\frac{1}{2}$	$\tilde{X}^2\Pi_{1/2g}$	0	$+\frac{1}{2}$	$+\frac{3}{2}$	$+\frac{1}{2}$
				+1	$-\frac{1}{2}$	$\tilde{A}^2\Pi_{1/2u}$	-2	$-\frac{1}{2}$	-1	-1	-2	$+\frac{1}{2}$	$-\frac{5}{2}$	-1	$-\frac{1}{2}$	$\tilde{X}^2\Pi_{3/2g}$	0	$-\frac{1}{2}$	$-\frac{3}{2}$	$-\frac{1}{2}$
			+1	$+\frac{1}{2}$	$\tilde{A}^2\Pi_{3/2u}$	-2	$-\frac{1}{2}$	0	-1	-1	$+\frac{3}{2}$	$-\frac{5}{2}$	+1	$+\frac{1}{2}$	$\tilde{X}^2\Pi_{3/2g}$	-2	$-\frac{1}{2}$	$+\frac{3}{2}$	$-\frac{5}{2}$	
			-1	$-\frac{1}{2}$	$\tilde{A}^2\Pi_{3/2u}$	+2	$+\frac{1}{2}$	0	+1	+1	$-\frac{3}{2}$	$+\frac{5}{2}$	-1	$-\frac{1}{2}$	$\tilde{X}^2\Pi_{3/2g}$	+2	$+\frac{1}{2}$	$-\frac{3}{2}$	$+\frac{5}{2}$	
			-1	$+\frac{1}{2}$	$\tilde{A}^2\Pi_{1/2u}$	+2	$-\frac{1}{2}$	0	+1	+1	$-\frac{1}{2}$	$+\frac{3}{2}$	-1	$+\frac{1}{2}$	$\tilde{X}^2\Pi_{1/2g}$	+2	$-\frac{1}{2}$	$-\frac{1}{2}$	$+\frac{3}{2}$	
			-1	$-\frac{1}{2}$	$\tilde{A}^2\Pi_{3/2u}$	+2	$-\frac{1}{2}$	-1	+1	0	$-\frac{3}{2}$	$+\frac{3}{2}$	-1	$-\frac{1}{2}$	$\tilde{X}^2\Pi_{3/2g}$	+2	$-\frac{1}{2}$	$-\frac{3}{2}$	$+\frac{3}{2}$	

might not ordinarily expect a Rydberg state with principal quantum number of 4 or 5 to be described by $\Omega_c\omega$ coupling, there is good evidence that this is indeed the case here. The most compelling evidence is that the intense members of the Tanaka-Ogawa Rydberg series converge to the $\tilde{A}^2\Pi_{1/2u}$ ion core, even for the very lowest members of this series; Tanaka

and Ogawa¹⁷ showed that the quantum defects are nearly constant for $m=4-11$. Furthermore, Cossart-Magos *et al.*⁷¹ showed that for series converging to $\tilde{X}^2\Pi_g$ the breakdown of ΛS coupling occurs at low to moderate n . We therefore conclude that the $m=5$ member of the Tanaka-Ogawa Rydberg series may be described by $\Omega_c\omega$ coupling and that

TABLE III. $\Omega_c \rightarrow \Omega^+$ selection rules for autoionizing transitions in ΛS coupling and $\Omega_c \omega$ coupling.

Ω	ΛS coupling notation	$\Omega_c \rightarrow \Omega^+$	Comments
		$(\pi_u)^3(\pi_g)^4\sigma_g \rightarrow (\pi_u)^4(\pi_g)^3 + \epsilon\sigma_u$	
$\Omega=2$	$^3\Pi_2$	$\Omega_c = \frac{3}{2} \rightarrow \Omega^+ = \frac{3}{2}$	(Dipole forbidden)
$\Omega=1$	$^{1,3}\Pi_1$	$\Omega_c = \frac{1}{2} \& \frac{3}{2} \rightarrow \Omega^+ = \frac{1}{2} \& \frac{3}{2}$	} ΛS coupling
$\Omega=1^-$		$\Omega_c = \frac{1}{2} \rightarrow \Omega^+ = \frac{1}{2}$	} $\Omega_c \omega$ coupling
$\Omega=1^+$		$\Omega_c = \frac{3}{2} \rightarrow \Omega^+ = \frac{3}{2}$	
$\Omega=0$	$^3\Pi_0$	$\Omega_c = \frac{1}{2} \rightarrow \Omega^+ = \frac{1}{2}$	(Forbidden in ΛS coupling; allowed in $\Omega_c \omega$ coupling)
		$(\pi_u)^3(\pi_g)^4\sigma_g \rightarrow (\pi_u)^4(\pi_g)^3 + \epsilon\delta_u$	
$\Omega=2$	$^3\Pi_2$	$\Omega_c = \frac{3}{2} \rightarrow \Omega^+ = \frac{1}{2}$	(Dipole forbidden)
$\Omega=1$	$^{1,3}\Pi_1$	$\Omega_c = \frac{1}{2} \& \frac{3}{2} \rightarrow \Omega^+ = \frac{1}{2} \& \frac{3}{2}$	} ΛS coupling
$\Omega=1^-$		$\Omega_c = \frac{1}{2} \rightarrow \Omega^+ = \frac{3}{2}$	} $\Omega_c \omega$ coupling
$\Omega=1^+$		$\Omega_c = \frac{3}{2} \rightarrow \Omega^+ = \frac{1}{2}$	
$\Omega=0$	$^3\Pi_0$	$\Omega_c = \frac{1}{2} \rightarrow \Omega^+ = \frac{3}{2}$	(Forbidden in ΛS coupling; allowed in $\Omega_c \omega$ coupling)
		$(\pi_u)^3(\pi_g)^4\delta_g \rightarrow (\pi_u)^4(\pi_g)^3 + \epsilon\delta_u$	
$\Omega=2$	$^3\Pi_2$	$\Omega_c = \frac{1}{2} \rightarrow \Omega^+ = \frac{1}{2}$	(Dipole forbidden)
$\Omega=1$	$^{1,3}\Pi_1$	$\Omega_c = \frac{1}{2} \& \frac{3}{2} \rightarrow \Omega^+ = \frac{1}{2} \& \frac{3}{2}$	} ΛS coupling
$\Omega=1^-$		$\Omega_c = \frac{1}{2} \rightarrow \Omega^+ = \frac{1}{2}$	} $\Omega_c \omega$ coupling
$\Omega=1^+$		$\Omega_c = \frac{3}{2} \rightarrow \Omega^+ = \frac{3}{2}$	
$\Omega=0$	$^3\Pi_0$	$\Omega_c = \frac{3}{2} \rightarrow \Omega^+ = \frac{3}{2}$	(Forbidden in ΛS coupling; allowed in $\Omega_c \omega$ coupling)
		$(\pi_u)^3(\pi_g)^4\delta_g \rightarrow (\pi_u)^4(\pi_g)^3 + \epsilon\sigma_u$	
$\Omega=2$	$^3\Pi_2$	$\Omega_c = \frac{1}{2} \rightarrow \Omega^+ = \frac{3}{2}$	(Dipole forbidden)
$\Omega=1$	$^{1,3}\Pi_1$	$\Omega_c = \frac{1}{2} \& \frac{3}{2} \rightarrow \Omega^+ = \frac{1}{2} \& \frac{3}{2}$	} ΛS coupling
$\Omega=1^-$		$\Omega_c = \frac{1}{2} \rightarrow \Omega^+ = \frac{3}{2}$	} $\Omega_c \omega$ coupling
$\Omega=1^+$		$\Omega_c = \frac{3}{2} \rightarrow \Omega^+ = \frac{1}{2}$	
$\Omega=0$	$^3\Pi_0$	$\Omega_c = \frac{3}{2} \rightarrow \Omega^+ = \frac{1}{2}$	(Forbidden in ΛS coupling; allowed in $\Omega_c \omega$ coupling)

autoionization proceeds via $\sigma_g \rightarrow \epsilon\sigma_u$ or via $\delta_g \rightarrow \epsilon\delta_u$. The conclusion that λ of the Rydberg electron does not change upon autoionization is in agreement with the results obtained for O₂.¹¹⁻¹³ Although the weight of the theoretical evidence (calculations of both intensity and quantum defects) would indicate that the Tanaka-Ogawa series is $nd\delta_g$, we seek additional evidence from the asymmetry parameter β to see if it is possible to decisively eliminate $ns\sigma_g$.

C. Energy dependence of the asymmetry parameter β

The off-resonance value of β for the $m=5$, (200) member of the Tanaka-Ogawa series shown in Fig. 4 is approximately -0.55 , which is in good agreement with several theoretical calculations.^{70,82-84} In the most recent of these, Dittman *et al.*⁷⁰ showed that the direct ionization cross section in the energy region shown in Fig. 4 (~ 16.72 eV) is composed of approximately equal contributions of σ_u and δ_u ionization continua; the σ_u contribution has 65% $l=1$ char-

acter and 35% $l=3$ character, and the δ_u contribution is dominated by $l=3$. Since no single angular momentum component is dominant, the off-resonance value of β does not exhibit the limiting geometric values of 0 ($f\delta$), -0.27 ($f\sigma$), or -0.40 ($p\sigma$).⁸⁵

Figure 4 shows that the on-resonance value of β for the $\tilde{X}(000)^2\Pi_{1/2g}$ spin-orbit component rises dramatically to a value of 0.4; the on-resonance value of β for the $\tilde{X}(000)^2\Pi_{3/2g}$ spin-orbit component shows no change from its off-resonance value. From the preceding discussion, we concluded that autoionization preserves the value of λ during decay; the most likely value of λ based on previous theoretical calculations is 2, which would lead to the ejection of an $f\delta$ partial wave if partial waves with $l=5$ and higher are neglected. Thus, if the photocurrent on resonance were due solely to the decay of the autoionizing resonance, we would expect to see an isotropic angular distribution ($\beta=0$) on resonance. We attribute the failure of the angular distribution to confirm this picture to the sizable background continuum,

which can spoil the single partial wave picture. Therefore, we may only tentatively conclude that the Tanaka–Ogawa Rydberg series is described by the electron configuration $\dots(\pi_u)^3(\pi_g)^4nd\delta_g^1\Pi_u$ in ΛS coupling or, more appropriately, by $\dots(\pi_u)^3(\pi_g)^4nd\delta_g\Omega=1^-$ in $\Omega_c\omega$ coupling. More detailed calculations of the asymmetry parameter that specifically include the effects of autoionization are required to confirm this conclusion.

A few other points can be made regarding the absolute values of β on and off resonance. The on-resonance value of β for the $\tilde{X}^2\Pi_{1/2g}$ spin–orbit component is significantly different from the off-resonance value. In particular, the large negative anisotropy observed off resonance gives way to a positive anisotropy on resonance. Since no calculation yet exists for this resonant process, further discussion of the variation of β within this resonance must be very speculative. In this discussion, we will use the angular momentum transfer picture for photoproduct angular distributions introduced by Dill and Fano.⁸⁶ In that picture, β is an incoherent sum of $\beta(j_i)$, weighted by the partial cross sections $\sigma(j_i)$, thus eliminating the interference terms present in an angular momentum representation. The angular momentum transferred in the photoionization process, j_t , is the vector sum of the angular momentum of the incoming photon and the angular momentum of the ejected electron. This sum is equal to the angular momentum transferred to the unobserved ionized molecule in the photoionization process. Of interest here is that there are at most three values of j_t for a particular ionization channel; each value is characterized by a well-defined set of angular momentum quantum numbers. Of these, j_t components for which j_t+1+j_γ is odd correspond to “parity-unfavored” transitions; those for which j_t+1+j_γ is even correspond to “parity-favored” transitions. The key point is that parity-unfavored transitions are characterized by $\beta=-1$. This is a geometric value, independent of dynamics. The value of β for parity-favored transitions is given by Eq. (12) of Ref. 86. This shows that it is possible for β to be negative under certain circumstances, but β for parity favored transitions is usually positive,⁸⁷ reaching the maximum value of $\beta=2$ in some well-known cases.

In the usual mechanistic picture, photoionization is broken into two stages—an initial stage of photoabsorption and a subsequent stage of escape of the photoelectron from the target. The first stage is characterized by parity-favored values of j_t ; parity-unfavored values of j_t are added to the photocurrent only as a result of anisotropic interactions experienced by the photoelectron as it escapes through the molecular field. The parity-unfavored components are characterized by $\beta=-1$, meaning that the photocurrent has a node along the polarization direction of the ionizing radiation and peaks perpendicular to this direction. Thus, the photoelectron escapes with an angular distribution signature opposite to that of the incoming radiation. This, in turn, implies that the anisotropy introduced into the excited complex by the incoming radiation remains in the residual ion. In parity-favored processes, the opposite is usually observed (though not rigorously required), and the photoelectron carries off the anisotropy brought into the process by the incident radiation.

The interesting point is that the present results exhibit a

counterintuitive behavior. Specifically, off-resonance, *direct* photoionization produces a β with a large negative value, usually indicating dominance by parity-unfavored component(s). On the other hand, *resonant* autoionization in this case produces positive values of β , which require parity-favored components. Of course, the observed behavior is not forbidden, because anisotropic forces are intrinsic to electron motion in a molecular field; rather, the observed behavior is just different from commonly invoked physical pictures. It would be very interesting to examine the details of a realistic calculation of this process to determine what produces the observed behavior and what physical picture best explains it. In this case, such a calculation would also help to definitively determine the value of λ for the Tanaka–Ogawa Rydberg series.

V. SUMMARY AND CONCLUSIONS

The spin–orbit dependence of angle- and energy-resolved photoelectron spectra was used to determine the electronic structure, symmetry, and decay dynamics of members of the Tanaka–Ogawa Rydberg series in CO₂. This represents the first time that spin–orbit selectivity has been used to obtain such information for a polyatomic molecule. The Tanaka–Ogawa Rydberg series in CO₂, which is assumed to have the electron configuration $\dots(\pi_u)^3(\pi_g)^4nd\delta_g$, was shown to autoionize primarily via a $d\delta_g \rightarrow \epsilon f\delta_u$ process when the totally symmetric vibronic components of the ion are produced. The Rydberg series appears to be well described by $\Omega_c\omega$ coupling, even for relatively low principal quantum numbers.

The interrogation of spin–orbit branching ratios and asymmetry parameters promises to be a quite versatile addition to the existing experimental techniques used to investigate the excited states of polyatomic molecules. Here, angle- and energy-resolved photoelectron spectroscopy was used to study the spectroscopy and decay dynamics of an autoionizing Rydberg state with diffuse rotational structure. It would also be of interest to study such a process as a function of principal quantum number. One might expect to see the photoelectron distribution change as the Rydberg state evolves from ΛS coupling to $\Omega_c\omega$ coupling with increasing principal quantum number (for example, from $^1\Pi_1$ and $^3\Pi_{0,1,2}$ states to $\Omega=2, 1^+, 1^-, 0$ states). Furthermore, the interrogation of spin–orbit branching ratios and asymmetry parameters should prove useful in multiphoton ionization studies of Rydberg states that lie below the first ionization threshold. Because such states cannot decay by autoionization, they are more likely to show well-resolved rotational structure. It should then be possible to study the direct ionization process as a function of both principal quantum number and rotational excitation. With resolved rotational structure, both Hund’s case (c) and Hund’s case (e) coupling limits may be observed. The latter has been developed to describe the departure from Hund’s case (c) coupling that accompanies j uncoupling of the Rydberg electron from the internuclear axis.^{81,88} In this limit, ω is no longer a good quantum number, but both Ω^+ and J^+ are well defined. Such studies could provide new information on the dynamics of the coupling in excited states.

ACKNOWLEDGMENTS

This work was supported by the U.S. Department of Energy, Office of Energy Research, Office of Health and Environmental Research, under Contract No. W-31-109-ENG-38, and by the Science and Engineering Research Council (U.K.). One of us (K.U.) wishes to thank the British Council for financial support.

- ¹M. A. Dillon, in *Creation and Detection of the Excited State*, edited by A. A. Lamola (Dekker, New York, 1971), Vol. 1, Part B, p. 375.
- ²P. J. Stephens, *Adv. Chem. Phys.* **35**, 197 (1976).
- ³P. R. Monson and W. M. McClain, *J. Chem. Phys.* **53**, 29 (1970).
- ⁴W. M. McClain, *J. Chem. Phys.* **55**, 2789 (1971).
- ⁵R. G. Bray and R. M. Hochstrasser, *Mol. Phys.* **31**, 1199 (1976).
- ⁶W. M. McClain and R. A. Harris, in *Excited States*, edited by E. C. Lim (Academic, New York, 1977), Vol. 3, p. 1.
- ⁷K.-M. Chen and E. S. Yeung, *J. Chem. Phys.* **69**, 43 (1978).
- ⁸D. L. Andrews and W. A. Ghoul, *J. Chem. Phys.* **75**, 530 (1981).
- ⁹M. A. C. Nascimento, *Chem. Phys.* **74**, 51 (1983).
- ¹⁰E. D. Poliakoff, J. L. Dehmer, A. C. Parr, and G. E. Leroi, *J. Chem. Phys.* **77**, 5243 (1982).
- ¹¹P. M. Guyon, J. W. Hepburn, T. Weng, F. Heiser, and D. Reynolds, *Phys. Rev. Lett.* **67**, 675 (1991).
- ¹²D. Čubrić, A. A. Wills, J. Comer, and M. Ukai, *Phys. Rev. Lett.* **71**, 983 (1993).
- ¹³D. Čubrić, A. A. Wills, J. Comer, and M. Ukai, *J. Phys. B* **26**, 3081 (1993).
- ¹⁴H. J. Henning, *Ann. Phys. (Leipzig)* **13**, 599 (1932).
- ¹⁵H. Sun and G. L. Weissler, *J. Chem. Phys.* **23**, 1625 (1955).
- ¹⁶Y. Tanaka, A. S. Jursa, and F. J. LeBlanc, *J. Chem. Phys.* **32**, 1199 (1960).
- ¹⁷Y. Tanaka and M. Ogawa, *Can. J. Phys.* **40**, 879 (1962).
- ¹⁸R. S. Nakata, K. Watanabe, and F. M. Matsunaga, *Sci. Light* **14**, 54 (1965).
- ¹⁹G. R. Cook, P. H. Metzger, and M. Ogawa, **44**, 2935 (1966).
- ²⁰J. A. R. Samson, J. L. Gardner, and J. E. Metall, *J. Geophys. Res.* **77**, 5560 (1972).
- ²¹L. C. Lee, R. W. Carlson, D. L. Judge, and M. Ogawa, *J. Quant. Spectrosc. Radiat. Transfer* **13**, 1023 (1973).
- ²²N. Wainfan, W. C. Walker, and G. L. Weissler, *Phys. Rev.* **99**, 542 (1955).
- ²³G. L. Weissler, J. A. R. Samson, M. Ogawa, and G. R. Cook, *J. Opt. Soc. Am.* **49**, 338 (1959).
- ²⁴V. H. Dibeler and J. A. Walker, *J. Opt. Soc. Am.* **57**, 1007 (1967).
- ²⁵K. E. McCulloh, *J. Chem. Phys.* **59**, 4250 (1973).
- ²⁶G. R. Parr and J. W. Taylor, *Int. J. Mass Spectrom. Ion. Phys.* **14**, 467 (1974).
- ²⁷G. G. Jones and J. W. Taylor, *J. Chem. Phys.* **68**, 1768 (1978).
- ²⁸J. Berkowitz, *Photoabsorption, Photoionization, and Photoelectron Spectroscopy* (Academic, New York, 1979).
- ²⁹S. H. Linn and C. Y. Ng, *J. Chem. Phys.* **75**, 4921 (1981).
- ³⁰P. M. Dehmer, *J. Chem. Phys.* **83**, 24 (1985).
- ³¹E. Lindholm, *Ark. Fys.* **40**, 125 (1969).
- ³²C. Fridh, L. Åsbrink, and E. Lindholm, *Chem. Phys.* **27**, 169 (1978).
- ³³M. I. Al-Joboury, D. P. May, and D. W. Turner, *J. Chem. Soc.* 6350 (1965).
- ³⁴D. W. Turner and D. P. May, *J. Chem. Phys.* **46**, 1156 (1967).
- ³⁵J. H. D. Eland and C. J. Danby, *Int. J. Mass Spectrom. Ion. Phys.* **1**, 111 (1968).
- ³⁶J. E. Collin and P. Natalis, *Int. J. Mass Spectrom. Ion. Phys.* **1**, 121 (1968).
- ³⁷C. R. Brundle and D. W. Turner, *Int. J. Mass Spectrom. Ion. Phys.* **2**, 195 (1969).
- ³⁸T. A. Carlson and G. E. McGuire, *J. Electron Spectrosc.* **1**, 209 (1972/73).
- ³⁹J. L. Gardner and J. A. R. Samson, *J. Electron Spectrosc.* **8**, 469 (1976).
- ⁴⁰A. W. Potts and G. H. Fattahallah, *J. Phys. B* **13**, 2545 (1980).
- ⁴¹V. Kumar and E. Krishnakumar, *J. Chem. Phys.* **78**, 46 (1983).
- ⁴²B. Kovac, *J. Chem. Phys.* **78**, 1684 (1983).
- ⁴³I. Reineck, C. Nohre, R. Maripuu, P. Lodin, S. H. Al-Shamma, H. Veenhuizen, L. Karlsson, and K. Siegbahn, *Chem. Phys.* **78**, 311 (1983).
- ⁴⁴B. Wannberg, H. Veenhuizen, L. Mattsson, K.-E. Norell, L. Karlsson, and K. Siegbahn, *J. Phys. B* **17**, L259 (1984).
- ⁴⁵H. Veenhuizen, B. Wannberg, L. Mattsson, K.-E. Norell, C. Nohre, L. Karlsson, and K. Siegbahn, *J. Electron Spectrosc.* **41**, 205 (1986).
- ⁴⁶L.-S. Wang, J. E. Reutt, Y. T. Lee, and D. A. Shirley, *J. Electron Spectrosc.* **47**, 167 (1988).
- ⁴⁷J. L. Bahr, A. J. Blake, J. H. Carver, and V. Kumar, *J. Quant. Spectrosc. Radiat. Trans.* **9**, 1359 (1969).
- ⁴⁸J. L. Bahr, A. J. Blake, J. H. Carver, J. L. Gardner, and V. Kumar, *J. Quant. Spectrosc. Radiat. Trans.* **12**, 59 (1972).
- ⁴⁹T. Gustafsson, E. W. Plummer, D. E. Eastman, and W. Gudat, *Phys. Rev. A* **17**, 175 (1978).
- ⁵⁰F. A. Grimm, J. D. Allen, Jr., T. A. Carlson, M. O. Krause, D. Mehaffy, P. R. Keller, and J. W. Taylor, *J. Chem. Phys.* **75**, 92 (1981).
- ⁵¹A. C. Parr, D. L. Ederer, J. L. Dehmer, and D. M. P. Holland, *J. Chem. Phys.* **77**, 111 (1982).
- ⁵²M.-J. Hubin-Franskin, J. Delwiche, P. Morin, M. Y. Adam, I. Nenner, and P. Roy, *J. Chem. Phys.* **81**, 4246 (1984).
- ⁵³M.-J. Hubin-Franskin, J. Delwiche, and P. M. Guyon, *Z. Phys. D* **5**, 203 (1987).
- ⁵⁴D. M. P. Holland, J. B. West, and M. A. Hayes, *Chem. Phys.* **148**, 241 (1990).
- ⁵⁵D. Villarejo, R. Stockbauer, and M. G. Inghram, *J. Chem. Phys.* **48**, 3342 (1968).
- ⁵⁶C. F. Batten, J. A. Taylor, and G. G. Meisels, *J. Chem. Phys.* **65**, 3316 (1976).
- ⁵⁷R. Frey, B. Gotchev, O. F. Kalman, W. B. Peatman, H. Pollak, and E. W. Schlag, *Chem. Phys.* **21**, 89 (1977).
- ⁵⁸R. Stockbauer, *Adv. Mass Spectrom.* **8A**, 79 (1980).
- ⁵⁹T. Baer and P. M. Guyon, *J. Chem. Phys.* **85**, 4765 (1986).
- ⁶⁰H. H. Fielding, T. P. Softley, and F. Merkt, *Chem. Phys.* **155**, 257 (1991).
- ⁶¹F. Merkt, S. R. Mackenzie, R. J. Rendall, and T. P. Softley, *J. Chem. Phys.* **99**, 8430 (1993).
- ⁶²See G. Chambaud, W. Gabriel, P. Rosmus, and J. Rostas, *J. Phys. Chem.* **96**, 3285 (1992), and references therein.
- ⁶³See, M. Brommer, G. Chambaud, E.-A. Reinsch, P. Rosmus, A. Spielfiedel, N. Feautrier, and H.-J. Werner, *J. Chem. Phys.* **94**, 8070 (1991), and references therein.
- ⁶⁴M. Johnson and J. Rostas (unpublished).
- ⁶⁵P. M. Dehmer, J. L. Dehmer, K. Ueda, J. B. West, M. R. F. Siggel, M. A. Hayes, and A. C. Parr (unpublished).
- ⁶⁶G. Herzberg, *Electronic Spectra and Electronic Structure of Polyatomic Molecules* (van Nostrand, Princeton, 1966).
- ⁶⁷P. M. Dehmer and J. L. Dehmer, *J. Chem. Phys.* **70**, 4574 (1979).
- ⁶⁸W. B. England and W. C. Ermler, *J. Mol. Spectrosc.* **85**, 341 (1981).
- ⁶⁹N. Padial, G. Csanak, B. V. McKoy, and P. W. Langhoff, *Phys. Rev. A* **23**, 218 (1981).
- ⁷⁰P. M. Dittman, D. Dill, and J. L. Dehmer, *Chem. Phys.* **78**, 405 (1983). Note that in Table II, the quantities in brackets were incorrectly denoted the high-*n* quantum defects, δ ; these quantities are actually $(1-\delta)$.
- ⁷¹C. Cossart-Magos, M. Jungen, and F. Launay, *Mol. Phys.* **61**, 1077 (1987).
- ⁷²W. B. England, W. C. Ermler, and A. C. Wahl, *J. Chem. Phys.* **66**, 2336 (1977).
- ⁷³A. C. Parr, S. H. Southworth, J. L. Dehmer, and D. M. P. Holland, *Nucl. Instrum. Methods* **222**, 221 (1984).
- ⁷⁴D. M. P. Holland, J. B. West, A. A. MacDowell, I. H. Munro, and A. G. Beckett, *Nucl. Instrum. Methods B* **44**, 233 (1989).
- ⁷⁵J. B. West and H. A. Padmore, in *Handbook on Synchrotron Radiation*, edited by G. V. Marr (North Holland, Amsterdam, 1987), p. 21.
- ⁷⁶P. M. Dehmer (unpublished).
- ⁷⁷G. V. Marr and J. B. West, *At. Data and Nucl. Data Tables* **18**, 497 (1976).
- ⁷⁸D. M. P. Holland, A. C. Parr, D. L. Ederer, J. L. Dehmer, and J. B. West, *Nucl. Instrum. Methods* **195**, 331 (1982).
- ⁷⁹R. Stockbauer, B. E. Cole, D. L. Ederer, J. B. West, A. C. Parr, and J. L. Dehmer, *Phys. Rev. Lett.* **43**, 757 (1979).
- ⁸⁰G. Herzberg, *Spectra of Diatomic Molecules* (van Nostrand, Princeton, 1950), p. 338.
- ⁸¹H. Lefebvre-Brion and R. W. Field, *Perturbations in the Spectra of Diatomic Molecules* (Academic, Orlando, 1986).
- ⁸²F. A. Grimm, T. A. Carlson, W. B. Dress, P. Agron, J. O. Thomson, and J. W. Davenport, *J. Chem. Phys.* **72**, 3041 (1980).
- ⁸³J. R. Swanson, D. Dill, and J. L. Dehmer, *J. Phys. B* **14**, L207 (1981).
- ⁸⁴R. R. Lucchese and V. McKoy, *Phys. Rev. A* **26**, 1406 (1982).
- ⁸⁵W. Thiel, *Chem. Phys.* **77**, 103 (1983).
- ⁸⁶D. Dill and U. Fano, *Phys. Rev. Lett.* **29**, 1203 (1972).
- ⁸⁷C. H. Greene and R. N. Zare, *Ann. Rev. Phys. Chem.* **33**, 119 (1982).
- ⁸⁸H. Lefebvre-Brion, *J. Chem. Phys.* **93**, 5898 (1990).